Ferromagnetism in 2D organic iron hemoglobin crystals based on nitrogenated conjugated micropore materials.

Ferromagnetism in 2D organic iron hemoglobin crystals based on nitrogenated conjugated micropore materials.

Artem Pimachev

Aerospace Mechanics Research Center

University of Colorado Boulder

Boulder, CO 80309

Robert D. Nielsen and Yuri Dahnovsky

Department of Physics and Astronomy/3905

1000 E. University Avenue

University of Wyoming

Laramie, WY 82071

Anri Karanovich

Department of Physics/0435

850 West Campus Drive

Virginia Polytechnic Institute and State University

Blacksburg, VA 24061

(Dated: October 31, 2019)

Abstract

In this work we study a low-cost two-dimensional ferromagnetic semiconductor with possible applications in biomedicine, solar cells, spintronics, and energy and hydrogen storage. From first principle calculations we describe the unique electronic, transport, optical, and magnetic properties of a π-conjugated micropore polymer (CMP) with three iron atoms placed in the middle of an isolated pore locally resembling heme complexes. This material exhibits strong Fe-localized d_{z^2} bands. The bandgap is direct and equal to $0.28\ eV$. The valence band is doubly degenerate at the Γ-point and for larger k-wavevectors the HOMO band becomes flat with low contribution to charge mobility. The absorption coefficient is roughly isotropic. The conductivity is also isotropic with the nonzero contribution in the energy range $0.3 - 8\ eV$. The xy-component of the imaginary part of the dielectric tensor determines the magneto-optical Faraday and Kerr rotation. Nonvanishing rotation is observed in the interval of $0.5 - 5.0\ eV$. This material is found to be a ferromagnet of an Ising type with long-range exchange interactions with a very high magnetic moment per unit cell, $m = 6\ \mu_B$. The exchange integral is calculated by two independent methods: (a) from the energy difference between ferromagnetic and antiferromagnetic states and (b) from a magnon dispersion curve. In the former case $J_{nn} = 27\ \mu eV$. In the latter case the magnon dispersion is fitted by the Ising model with the nearest and next-nearest neighbor spin interactions. From these estimations we find that $J_{nn} = 19.5\ \mu eV$ and $J_{nnn} = -3\ \mu eV$. Despite the different nature of the calculations, the exchange integrals are only within 28% difference.

I. INTRODUCTION

Two-dimensional (2D) materials have attracted a great deal of attention due to their unusual electronic, transport, optical, and magnetic properties.[1,2] Graphene, as a pioneer of 2D materials, possesses a high carrier mobility up to 105 $cm^2/(Vs)$ due to the massless Dirac cone, having a potential in electronic applications, such as RF transistors and inverters.[3,4] Recently, the discovery of magnetism in 2D crystals opens opportunities for 2D magnetic, magneto-electric and magneto-optic devices.[5,6] However, layered materials with intrinsic ferromagnetic (FM) and semiconducting characteristicss are difficult to realize around room temperature. For instance, all the FM transition metal dichalcogenides (TMDCs) are metallic[7] and only some types of 2D materials such as transition-metal trichalcogenides (TMTCs) $CrXTe_3$ (X = Si, Ge and Sn)[8,9] and chromiumtrihalides CrA_3 (A = F, Cl, Br and I)[10] have been reported as intrinsic FM semiconductors. Such ferromagnetic semiconductors are unstable in the environment and degrade in several minutes changing their properties.[11] In this work we theoretically propose a new 2D organic ferromagnetic semiconductor that is supposed to be more stable to oxygen and other gases in air. We calculate electronic, transport, optical, and magnetic properties of such a ferromagnet. The design of the two-dimensional crystal is based on π-conjugated microporous polymers (CMPs). Such materials have a nitrogenated porous structure[12] with multiple benzene rings on a side of a hexagonal unit cell. The repeated structure results in a novel class of extended porous frameworks, which are known as π-conjugated microporous polymers. Aza-CMP[13,14], with the direct bandgap of *1.65 eV*[15], is promising for an electric power supply and for efficient energy storage.[16] It has been shown that the band-gap can be tuned from *1.64* to *0.96 eV* by replacing hydrogens by halogen substituents varying from fluorine to iodine.[17] Indeed, the applications of the nitrogenated microporous materials are very broad. They can be useful as sensitizers in solar cells[18], for water splitting catalysis[19], in biomedicine[20], as a photocatalyst[15], and for gas storage and separation[21]. If we insert into one of the pores three locally heme-like structures we obtain the 2D crystal structure shown in Fig. 1a.

If we look carefully at the structure of iron atoms inside the nitrogenated ring, we find that it resembles myoglobin or hemoglobin where an iron atom is bonded to four nitrogen atoms as shown in Fig. 1b. In this work we study the electronic, optical, transport, and magnetic properties of such a 2D crystal.
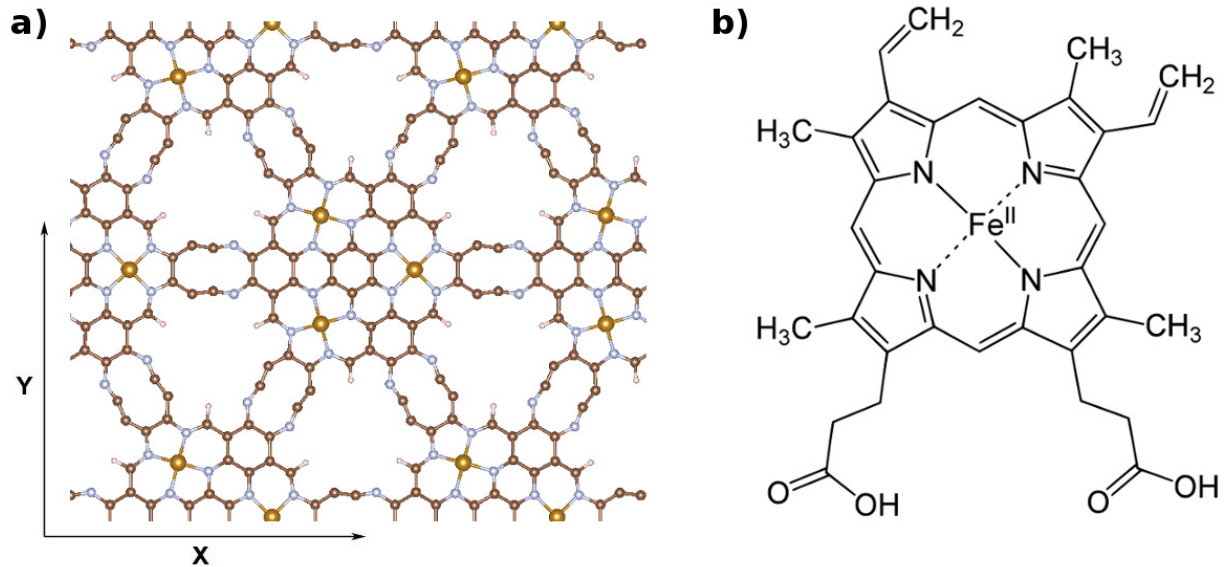
FIG. 1: Crystal structures of (a) the nitrogenated porous materials with three iron atoms inside the six-benzene-ring-CMP unit cell, Fe-CMP, and (b) a heme group b molecule with an iron atom bound to the four nitrogen atoms. The ions in (a) are brown for carbon, blue for nitrogen, red for hydrogen, and bronze for iron. Each unit cell contains 75 total atoms consisting of one iron cluster of the larger hexagonal aza-CMP structure.

II.   COMPUTATIONAL DETAILS

Electronic structure calculations and geometry optimizations have been performed within the density functional theory (DFT) with the generalized gradient approximation (GGA) using the Vienna Ab-initio Simulation Package (VASP).[22] Projector augmented plane-wave (PAW) pseudopotentials with a cutoff energy of 400 eV have been employed for the calculations.[23] A Γ-centered k-point grid has been generated from the Monkhorst-Pack scheme.[24] The vacuum space between the surfaces has been chosen to be around 10 $\mathring{A}$ to avoid interaction between 2D periodic surfaces. The structure relaxation has been performed with the Pedrew-Burke-Ernzerhof (PBE) exchange-correlation functional and a $4 \times 4 \times 1$ k-mesh grid using the conjugate gradient algorithm.[25] The band structure, density of states, and absorption spectra for these materials have been calculated with a $16 \times 16 \times 1$ k-mesh grid. For the band structure calculations we have used the M-Γ-K-M path in a k-space. For the calculations along this path we have chosen 40 k-points in total.

Using VASP we have calculated the frequency-dependent dielectric tensor $\varepsilon(E)$ using the independent particle approximation (IPA) to determine the absorption coefficient tensor. For magnetic calculations the exchange integral has been estimated from two independent methodologies: (a) as a difference in the ferromagnetic (FM) and anti-ferromagnetic (AFM) energies and (b) from the calculations of the magnon dispersion curve. Anti-ferromagnetic calculations were carried out using each iron center as a magnetic unit to investigate long-range magnetic ordering. To do so, 4 iron clusters were used such that each corner of the super-cell anti-ferromagnetically coupled with it's 2 nearest neighbors. For materials such as this, pure GGA exchange-correlation based DFT erroneously estimates magnetic properties. To overcome this, we employ DFT+U with a Hubbard term of U = 5 eV which has been shown to correctly describe the magnetic properties of iron porphyrins.[26]

III. ELECTRONIC PROPERTIES

The 2D Fe-CMP crystal depicted in Fig. 1a is a novel material, which geometries and electronic properties are unknown. Thus, we first study its crystal structure. After the geometric optimization we have found that the crystal structure is hexagonal with the following crystal unit lattice constants: $a = 17.1018$ $\mathring{A}$ and $b = 17.1019$ $\mathring{A}$ and angles $\alpha = 90.11°$ and $\beta = 88.08°$. The electronic structure of the crystal depends on a multiplicity of a unit cell. To determine the multiplicity of the ground state we have used the QUANTUM ESPRESSO software package[27] with the same cutoffs and functionals listed in *Computational Details*. To accurately evaluate the multiplicity, broken-symmetry DFT was utilized. The minimum ground-state multiplicity energy was found to be $M = 7$ with VASP. To confirm this, multiplicities from $M = 1$ to $M = 13$ were calculated. Odd multiplicities were chosen to minimize computational costs however there is a possibility that there might be an energy minimum at an odd multiplicity. The ground state energies for various multiplicities are shown in Fig. 2. From the symmetry of the multiplicity curve it is evident that the minimum multiplicity $M = 7$, as was found in VASP.

We have also calculated the density of states depicted in Fig. 3b and c for the crystal presented in Fig. 1a. We see that the energy gap is about 0.28 eV. A strong localized band is demonstrated from the calculations. The theoretical analysis indicates that this band is
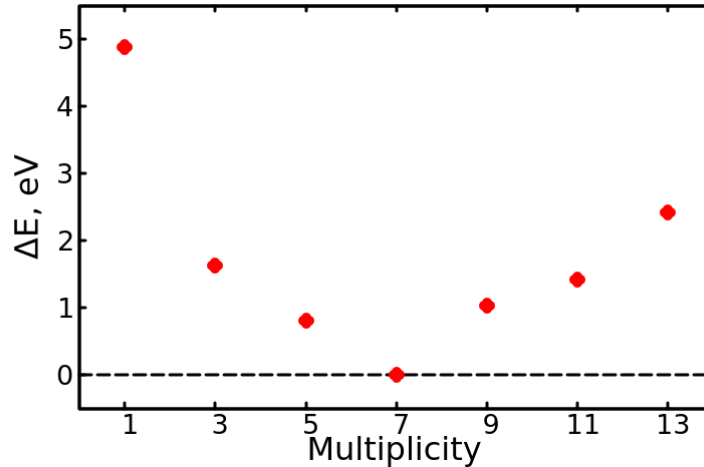
FIG. 2: Energy dispersion of different multiplicities of the crystal unit cell.

due to d_{z^2} iron orbitals. To prove this we have calculated the density of states (DOS) of the same material but without iron atoms while keeping the geometry unchanged. The DOS for the latter material is depicted in Fig. 3a. Despite the optimization of the structure we see that the strong localized band disappears. Thus, we conclude that this band is due to the presence of the iron atoms. The width of the band is $0.011\ eV$. To further demonstate that this strongly localized band is the d_{z^2} orbital, we provide the PDOS of the orbital compared to the total DOS in Fig. 3c. Indeed, the strongly localized band is made of the d_{z^2} orbital of the iron atoms.

From the charge distribution, presented in Fig. 4, we see that charges on the iron atoms are strongly localized while the charges in the rest of the Fe-CMP are very delocalized. The strongly localized nature of the charges on the iron atoms allow us to estimate the total charge occupation. For iron atoms, it is found that the total occupation of $d-$electrons is 6.3. This value is consistent with other studies of porphyrin molecules.[28] The remaining charge distribution is uniformly distributed over the surrounding molecules. The total charge of the Fe-CMP is neutral.

In addition, we have calculated the band structure. From Fig. 5 we see that the band-gap is direct and centered at the Γ-point. The localized Fe-band is flat and shown by the straight lines. From this figure we see that the valence band is doubly degenerate at the Γ-point. The effective masses are much smaller for holes than for electrons. It is important to mention that at other symmetry points (K and M) the valence band becomes
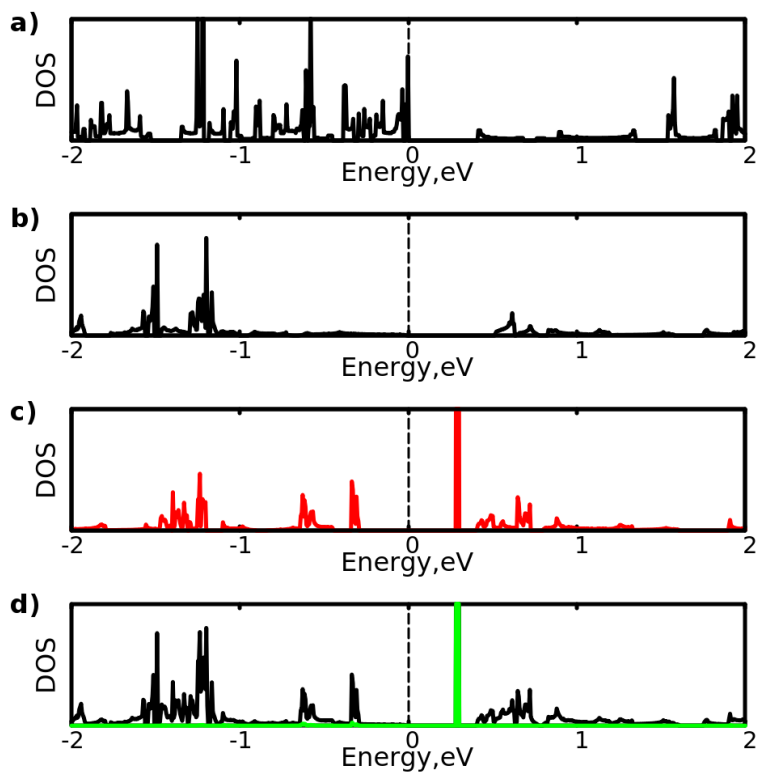
FIG. 3: Density of states (DOS) for (a) the aza-CMP structure, (b) the Fe-CMP spin "down" projected DOS, and (c) the Fe-CMP spin "up" projected DOS, and (d) the total DOS for the Fe-CMP compared to the d_{z^2} orbital.
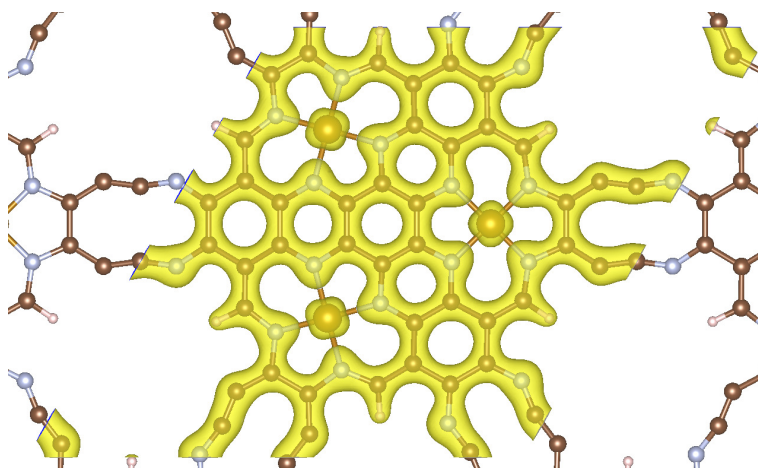

FIG. 4: Charge distribution of the Fe-CMP.

a Fe-localized flat band. This means that the efficient mobility in k-space is restricted in the vicinity of the Γ-point.
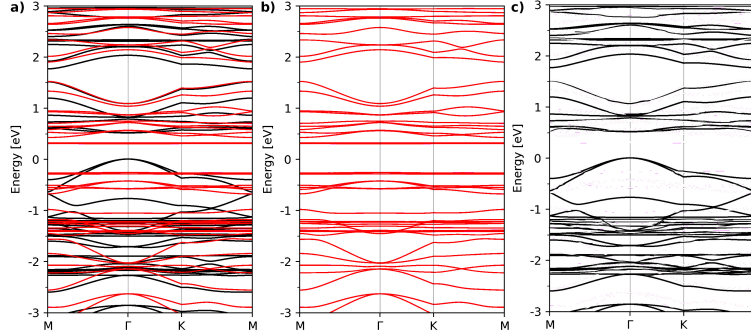

FIG. 5: (a) Spin projected band structure of the Fe-CMP where red bands are the spin "down" projections and black bands are the spin "up" projections, (b) band structure for spin "down" projections, and (c) band structure for spin "up" projections.

IV. OPTICAL PROPERTIES

The absorption spectrum has been obtained from the VASP calculations using the IPA method where absorption coefficient has been found from the imaginary part of a dielectric tensor ($\alpha = \frac{\omega}{nc} Im(\epsilon)$) as shown in Fig. 6. Figs. 6a, b, and c represent α_{xx}, α_{yy}, and α_{xy}, respectively. We see that the absorption in x- and y-directions are almost equal. As shown from these figures, the iron band almost does not contribute to the absorption due to its very small width. The xy-component describes magneto-optical (Kerr and Faraday) effects. For example, the Faraday rotation angle is $\theta_F = \omega\, d\, Im(\varepsilon_{xy})/2nc$[29], where n is a refractive index in the direction of propagation, c is a speed of light, and d is a propagation distance. Fig. 6c demonstrates that the Faraday rotation is substantial in the energy interval $0.5 - 3\ eV$. The Kerr rotation angle $\phi_K = Im(\varepsilon_{xy})/(\sqrt{\varepsilon_{xx}}(1 - \varepsilon_{xx}))$[30] is also proportional to $Im(\varepsilon_{xy})$ shown in Fig. 6c.
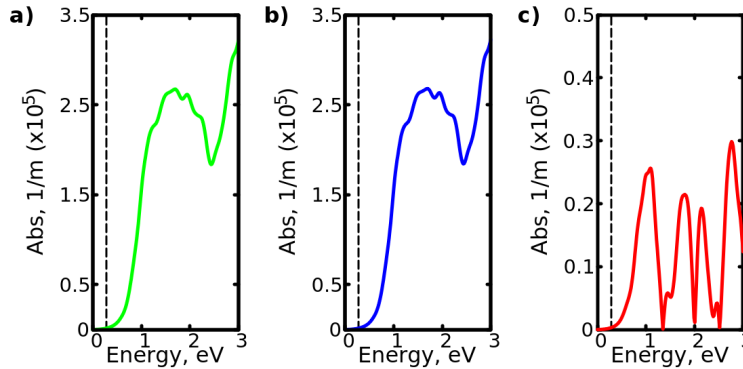
FIG. 6: Absorption coefficients for different directions of the Fe-CMP structure. The directional components are for the (a) xx-component, (b) yy-component, and (c) xy-component.

V.   TRANSPORT PROPERTIES

Transport properties are isotropic resembling the absorption spectra. The conductivity is calculated from the following equation: $\sigma(\omega) = \frac{\alpha(\omega)n(\omega)c}{4\pi}$, where n is the index of refraction in the direction of the conduction. We demonstrate the energy dependences of the conductivity tensor for different components in Fig. 7. As we see the σ_{xx} and σ_{yy} are similar. There is a significant conduction for the energies between $0.3 - 8\ eV$. The xy-component of the conductivity, which is in charge of a Hall effect is negligibly small.

VI.   MAGNETIC PROPERTIES

From the electronic structure calculations we have found that the Fe-CMP is a ferromagnet. The calculations have been performed in a zero magnetic field. Such a condition excludes the possibility of superparamagnetism at zero temperature. The ferromagnetic behavior of the crystal is due to the exchange interaction between neighboring iron clusters. Thus, we consider the iron clusters as our unit spin. The iron clusters in the middle of the CMP structure have a total magnetic moment $m = 6\ \mu_B$. The magnetic moment direction (z-direction) is perpendicular to the crystal plane. Taking this into account, we describe the ferromagnetism in terms of the Ising model. Because the iron clusters are far separated from each other, we expect the exchange integral to be small. To
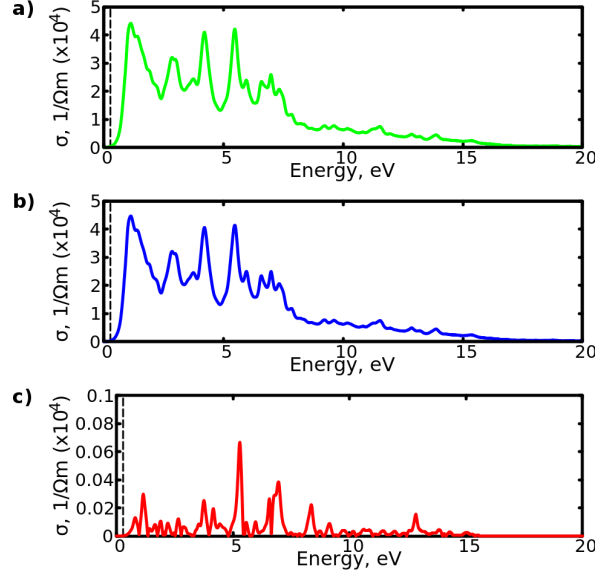
FIG. 7: The conductivity tensor of the Fe-CMP for the (a) xx-component, (b) yy-component, and (c) xy-component.

determine the exchange integral in the Ising model we have used the following procedure. First, we have found the ground state energy of the ferromagnetic state with $M = 7$. Second, we have determined the energy in the antiferromagnetic state where we flip the spin of the neighboring iron cluster(s) as a whole unit. In our calculation we have used a supercell of four iron clusters with a vanishing total magnetic moment. From the difference in energy between the ferromagnetic and antiferromagnetic ground state energies we determine the exchange integral using the Ising model Hamiltonian energy. From the VASP calculations we have found the exchange integral between the nearest neighbors to be $J_{nn} = 27$ μeV. To make sure that our estimations are correct we have used another independent methodology to determine the exchange integral. Employing the spin-spiral option in VASP we have calculated the magnon dispersion energies for different in-plane wavevectors. For example, for the [100] direction the magnon dispersion curve is shown in Fig 8. To estimate the value of the exchange integral we have fitted the following equation based on the Ising model for the nearest and next nearest neighbors, $\Delta E_{Magnon} = 2S[6J_{nn} + 12J_{nnn} - J_{nn}\Sigma cos(\vec{q} \cdot \vec{R}_{nn}) - J_{nnn}\Sigma cos(\vec{q} \cdot \vec{R}_{nnn})$.[31] The calculated energy values for each spin-spiral wavevector in the [100] direction is shown in Fig. 8. The red dashed line represents the computed magnon dispersion curve while the black solid

10

line describes the fitted magnon dispersion dependence. The best fitting for the calculated dispersion provides the following exchange integrals: $J_{nn} = 19.5~\mu eV$ and $J_{nnn} = -3~\mu eV$. Despite the different nature of the calculations, the exchange integrals are only within 28% difference. The discrepancy may due to the fact that the former method includes the estimations of J for the spin nearest-neighbors in the Ising model while the later method provides the best fit for the calculations where additionally we have added the next-nearest neighbors. Thus, the two methods are not entirely equivalent. The exchange interaction represents a long-range ferromagnetic ordering between iron clusters in the 2D CMP crystal. We consider, also, the possible effects of dipole-dipole interactions between iron clusters. However, due to the large distances between the clusters, we find from direct estimates that the energy contribution of dipole-dipole interactions are about 200 times lesser than the observed energy differences between magnetic states.
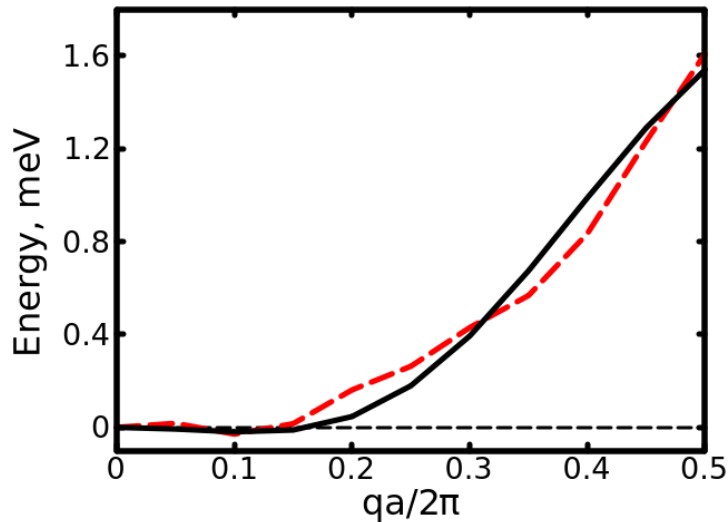

FIG. 8: Magnon dispersion of the Fe-CMP along the [100] direction. The solid black line is the fitted magnon dispersion curve and the dashed red line is the calculated energy of the magnon.

VII. CONCLUSIONS

In this work we have studied 2D ferromagnetic semiconducting CMPs with an isolated cluster of three iron atoms locally resembling heme complexes presented in Fig. 1a. We

have shown that this material is ferromagnetic with a very high magnetic moment per unit cell, $m = 6$ μ_B, with a long-range exchange interaction. In addition to the magnetic moment, we have determined the magnon dispersion curve shown in Fig. 8, from which we have estimated long-range exchange integrals between iron clusters, $J_{nn} = 19.5$ μeV and $J_{nnn} = -3$ μeV. Furthermore, we have determined the DOS shown in Fig. 3 and the band structure depicted in Fig. 5. Both the DOS and band structures indicate a strongly localized band as proved to be due to the d_{z^2} iron orbitals. Interestingly, the valence band determines the carrier dynamics by lighter holes with k-wavevectors in the vicinity of the Γ-point. For other symmetry points (K and M) the dispersion curve is flat due to the Fe-localized band with vanishing hole velocities. Optical absorption is independent of the direction of light propagation. We have also calculated ε_{xy} which determines the Faraday and Kerr rotation angles. As shown in Fig. 6c the rotation angles are pronounced in the energy range of $0.5 - 3eV$. Besides electronic, optical, and magnetic properties we have also studied transport properties calculating the conductivity tensor. The conductivity tensor is similar for the x- and y-direction. The main conductivity is in the energy range of $0.3 - 8$ eV. We have also calculated the xy-component of the conductivity tensor which appears to be very small indicating a small Hall effect.

This material has great potential in a wide range of possible applications. The high magnetic moment per unit cell and long-range ferromagnetic ordering allows the possibility to be employed as an auxiliary material for spintronics, its semiconducting nature can be used to sensitize solar cells, the crystals resemblance to the heme-complex allows for its application in biomedicine, and the large porous nature allows for the implementation in gas separation and storage.

Acknowledgments

---

[1] K. S. Novoselov, A. K. Geim, S. V. Morozov, D. Jiang, Y. Zhang, S. V. Dubonos, I. V. Grigorieva, and A. A. Firsov, *Science*, 2004, **306**(5696), 666–669.

[2] M. Xu, T. Liang, M. Shi, and H. Chen, *Chemical Reviews*, 2013, **113**(5), 3766–3798.

[3] S. Morozov, K. Novoselov, M. Katsnelson, F. Schedin, D. Elias, J. A. Jaszczak, and A. Geim, *Physical Review Letters*, 2008, **100**(1), 016602.

[4] F. Schwierz, *Nature Nanotechnology*, 2010, **5**(7), 487.

[5] C. Gong, L. Li, Z. Li, H. Ji, A. Stern, Y. Xia, T. Cao, W. Bao, C. Wang, Y. Wang, et al., *Nature*, 2017, **546**(7657), 265.

[6] B. Huang, G. Clark, E. Navarro-Moratalla, D. R. Klein, R. Cheng, K. L. Seyler, D. Zhong, E. Schmidgall, M. A. McGuire, D. H. Cobden, et al., *Nature*, 2017, **546**(7657), 270.

[7] C. Ataca, H. Sahin, and S. Ciraci, *The Journal of Physical Chemistry C*, 2012, **116**(16), 8983–8999.

[8] X. Li and J. Yang, *Journal of Materials Chemistry C*, 2014, **2**(34), 7071–7076.

[9] H. L. Zhuang, Y. Xie, P. Kent, and P. Ganesh, *Physical Review B*, 2015, **92**(3), 035407.

[10] W.-B. Zhang, Q. Qu, P. Zhu, and C.-H. Lam, *Journal of Materials Chemistry C*, 2015, **3**(48), 12457–12468.

[11] M. Yu, X. Liu, and W. Guo, *Physical Chemistry Chemical Physics*, 2018, **20**(9), 6374–6382.

[12] M. Bieri, M. Treier, J. Cai, K. Aït-Mansour, P. Ruffieux, O. Gröning, P. Gröning, M. Kastler, R. Rieger, X. Feng, K. Müller, and R. Fasel, *Chem. Commun.(Cambridge)*, 2009, **45**, 6919.

[13] Z.-D. Yang, W. Wu, and X. C. Zeng, *Journal of Materials Chemistry C*, 2014, **2**(16), 2902–2907.

[14] V. Briega-Martos, A. Ferre-Vilaplana, A. de la Pena, J. L. Segura, F. Zamora, J. M. Feliu, and E. Herrero, *ACS Catalysis*, 2016, **7**(2), 1015–1024.

[15] L. Wang, Y. Wan, Y. Ding, Y. Niu, Y. Xiong, X. Wu, and H. Xu, *Nanoscale*, 2017, **9**(12), 4090–4096.

[16] Y. Kou, Y. Xu, Z. Guo, and D. Jiang, *Angewandte Chemie*, 2011, **123**(37), 8912–8916.

[17] A. Pimachev, V. Proshchenko, and Y. Dahnovsky, *Journal of Applied Physics*, 2017, **122**(11), 115305.

[18] S. Fukuzumi, Y.-M. Lee, and W. Nam, *Chemistry–A European Journal*, 2018, **24**(20), 5016–5031.

[19] L. Wang, X. Zheng, L. Chen, Y. Xiong, and H. Xu, *Angewandte Chemie International Edition*, 2018, **57**(13), 3454–3458.

[20] T. T. Lee and R. L. Momparler, *Analytical Biochemistry*, 1976, **71**(1), 60–67.

[21] A. Pimachev and Y. Dahnovsky, *Journal of Applied Physics*, 2018, **124**(19), 194303.

[22] G. Kresse and J. Furthmüller, *Computational Materials Science*, 1996, **6**(1), 15–50.

[23] P. E. Blöchl, *Physical Review B*, 1994, **50**(24), 17953–17979.

[24] H. J. Monkhorst and J. D. Pack, *Physical Review B*, 1976, **13**(12), 5188.

[25] J. P. Perdew, K. Burke, and M. Ernzerhof, *Physical Review Letters*, 1996, **77**(18), 3865–3868.

[26] D. A. Scherlis, M. Cococcioni, P. Sit, and N. Marzari, *The Journal of Physical Chemistry B*, 2007, **111**(25), 7384–7391.

[27] P. Giannozzi, S. Baroni, N. Bonini, M. Calandra, R. Car, C. Cavazzoni, D. Ceresoli, G. L. Chiarotti, M. Cococcioni, I. Dabo, et al., *Journal of Physics: Condensed Matter*, 2009, **21**(39), 395502.

[28] M. P. Johansson and D. Sundholm, *The Journal of Chemical Physics*, 2004, **120**(7), 3229–3236.

[29] F. Oliveira, *DOI: 10.13140/RG.2.1.1319.6881*.

[30] W.-S. Kim PhD thesis, Universität Duisburg-Essen, 1998.

[31] J. Van Kranendonk and J. Van Vleck, *Reviews of Modern Physics*, 1958, **30**(1), 1.